Experimental and numerical simulation of pits on a corroded 316L grade stainless steel

E. SASSINE[1], J. ROSEC[2], V. BRUYERE[1], R. FARGERE[2], P. NAMY[1]

[1]SIMTEC, 5 rue Felix Poulat, 38000 Grenoble, France

[2] Naval Group– CESMAN, Technocampus Océan – 5 rue de l'Halbrane, 44340 Bouguenais, France

Abstract

Corrosion is an ongoing issue in metallurgic field. Stainless-steel products are likely to corrode in certain environmental conditions, especially if they are exposed to marine environment where localized corrosion can occur. The aim of this work is to study the behavior of 316L grade stainless steel subjected to pitting corrosion in a marine solution. The originality of this paper is that chemical kinetics parameters used in numerical simulation are based on experimental campaign in artificial seawater. Pitting initiation mechanism is not be treated in this paper and the main interest is focused on pits development. 2D Axisymmetric simulations in transient mode were accomplished thanks to COMSOL Multiphysics® software. The analysis of the experimental measurements indicates that mean width and depth of pits are relatively close, so pits can be considered as a hemisphere. Numerical results show that pit propagation depends on its initial form. A hemispherical pit keeps its shape during propagation (only its radius increases over time) while an ellipsoid pit has a different behavior.

I. Introduction

Pitting corrosion is a main form of so-called localized corrosion. It produces microcavities on the surface of the depassivated material which gradually get deeper. Thus, for localized pitting corrosion, most of the existing models describe the propagation phase of the pitting in potenstiostatic mode. Laycock [1] has developed a 2D model using the finite element method. His model details anodic dissolution kinetics and proposes a critical current density for repassivation which varies with the local concentration of corrosion products. S. Scheiner and Hellmich [2] provide 1D and 2D finite volume models with two dissolution regimes, depending on whether the solution is saturated or not: the first regime governed by Arrhenius-type activation and the second by the diffusion of ionic species. Zhu et al. [3] developed a model of pitting growth for petroleum pipelines in sweet (CO_2) production environments. Mai et al. [4] proposed an original numerical approach, using the "phase-field" method to describe numerically the solid/liquid interface close to the pit. The model can reproduce the different portions of the polarization curve of the material, associated with the corrosion regimes (activation, diffusion, or mixed regime). It has also been applied to identify the interaction between different pits, and to study the corrosion of composite materials and polycrystalline steels. Thesis work has been undertaken to numerically simulate the propagation of pitting on carbon steels (Salleh [5]) or iron in a chlorinated environment (Tricoit [6]). This results in 2D single-pit corrosion models applied to several environment of different salinity and chemical composition, taking into consideration the precipitated phases. Pitting corrosion models applied to nickel-based steel alloys were developed by Xiao et al. [7] with respect to pit shape, corrosion current and the influence of chloride ions. Wang and Han [8] modelled the pitting interactions generated by the chemical-mechanical stress of a stainless steel, showing in particular an accelerating effect of corrosion in the case of pitting coalescence. Their study also showed the effect of the mechanical load position on the pitting evolution. The aim of this work is to study the behavior of 316L grade stainless steel subjected to pitting corrosion in a marine solution using numerical simulation. Pit's shape effect will also be discussed by considering an ellipsoid and a hemispherical pit, respectively.

II. Numerical Model

Numerical simulations were accomplished thanks to COMSOL Multiphysics® software using a 2D-axisymmetric model in transient mode. This numerical model consists in solving both mass conservation equation and charge conservation equation. For this reason, "Corrosion, Tertiary with Electroneutrality interface" was used to describe transport of species (ions) in the electrolyte, current distribution, and geometrical changes of the pit. In the absence of convection, the transport of a species "i" in an electrolyte is given by (**Eq.1**):

$$N_i = -D_i.\nabla c_i - z_i.u_i.F.c_i\nabla\varphi_L \qquad \textbf{Eq.1}$$

with :

- z_i: charge number of the species.
- u_i: mobility of the species given by the Nernst-Einstein relation $D_i/(R.T)$, with R ideal gas constant (8,314 $J.mol^{-1}.K^{-1}$) and T the temperature (298 K, corresponding to 25°C).
- F: Faraday constant (96485 $C.mol^{-1}$).
- c_i : concentration ($mol.m^{-3}$).
- φ_L : electrostatic potential of the solution (V).

- D_i: diffusion coefficient ($m^2.s^{-1}$) of each chemical species, as presented in **Table. 1** below:

chemical species	Na^+	Cl^-	Fe^{2+}	H^+	OH^-
D_i ($m^2.s^{-1}$)	1,33. 10^{-9}	2,03. 10^{-9}	7,1. 10^{-10}	9,3. 10^{-9}	5,3. 10^{-9}
chemical species	$FeOH^+$	O_2	Cr^{3+}	$Cr(OH)^{2+}$	
D_i ($m^2.s^{-1}$)	7,5. 10^{-10}	2,4. 10^{-9}	1,78. 10^{-9}	7,3. 10^{-10}	

Table. 1 - Diffusion coefficient for chemical species

Thus, at the stationary state, the mass balance equation (also called the Nernst-Planck equation) can be expressed as follows (**Eq.2**):

$$\nabla . N_i = R_i \qquad \textbf{Eq.2}$$

With "R_i" the rate of homogeneous chemical reaction per unit volume (**Table. 2**): kinetic constants in the " forward " direction (k_f) and in the " backward " direction (k_b) were used.

Reactions			
$a_i=c_i/c_0$: activity of species i, $c_0=10^3$ mol.m^{-3}			
Equations	k_f	k_b	$K_{eq}=k_f/k_b$
Homogeneous reactions, T=25 °C			
$R_w = k_{wf} - k_{wb}.a_{H^+}.a_{OH^-}$	10 mol.m^{-3}s^{-1}	10^{15} mol.m^{-3}s^{-1}	10^{-14}
	$H_2O \underset{k_{wb}}{\overset{k_{wf}}{\rightleftharpoons}} H^+ + OH^-$		
$R_{FeOH} = k_{FeOH^+f}.a_{Fe^{2+}} - k_{FeOH^+b}.a_{FeOH^+}.a_{H^+}$	3.10^3 mol.m^{-3}s^{-1}	9,5.10^{12} mol.m^{-3}s^{-1}	$10^{-9,5}$
	$Fe^{2+} + H_2O \underset{k_{FeOH^+b}}{\overset{k_{FeOH^+f}}{\rightleftharpoons}} FeOH^+ + H^+$		
$R_{Cr(OH)^{2+}f} = k_{Cr(OH)^{2+}f}.a_{Cr^{3+}} - k_{Cr(OH)^{2+}b}.a_{Cr(OH)^{2+}}.a_{H^+}$	8.10^4 mol.m^{-3}s^{-1}	2,1.10^8 mol.m^{-3}s^{-1}	$10^{-3,42}$
	$Cr^{3+} + H_2O \underset{k_{Cr(OH)^{2+}b}}{\overset{k_{Cr(OH)^{2+}f}}{\rightleftharpoons}} Cr(OH)^{2+} + H^+$		

Table. 2 - R_i value for homogeneous reactions

Moreover, the electrostatic potential of the solution is also an unknown factor verifying the Poisson equation expressed by (**Eq.3**):

$$\vec{\nabla}^2 \varphi_L = -\frac{F}{e}\sum_i z_i . c_i \qquad \textbf{Eq.3}$$

It should be noted that "e" represents the dielectric permittivity of the medium (7,08.10^{-11} F.m^{-1} at 25°C) and the ratio "F/e" of the equation is very large, of the order of 10^{15} at 25°C, so that the hypothesis of the electroneutrality of the electrolyte (medium), given by **Eq.4** , can be verified :

$$\sum_i z_i . c_i = 0 \qquad \textbf{Eq.4}$$

Geometry

A 2D Axisymmetric (rotational symmetry around the "Z" axis) geometry with single corrosion pit will be considered in all numerical simulations. Corrosion pit had an ellipse shape with "a" and "b" as semi-major and semi-minor axis, respectively. In total, three corrosion pits with two different shapes will be tested:

a) Ellipsoid pit with a=100 µm and b=5µm

b) Two Hemispherical pits with a radius of 5 and 100µm, respectively

Different boundaries shown in **Figure 1** represent:

- **(1)**: electrolyte limit whose radius is equal to 5mm
- **(2)**: active part of the external surface, where oxygen reduction is taking place. The length of this part is about 4mm.
- **(3)**: pit boundary known also as active site of 316L steel, where steel oxidation is taking place.
- **(4)**: diffusion zone boundary noted δ, fixed at 500 µm in all study cases.
- **(5)**: inactive part of the external surface (electrochemically insulating)

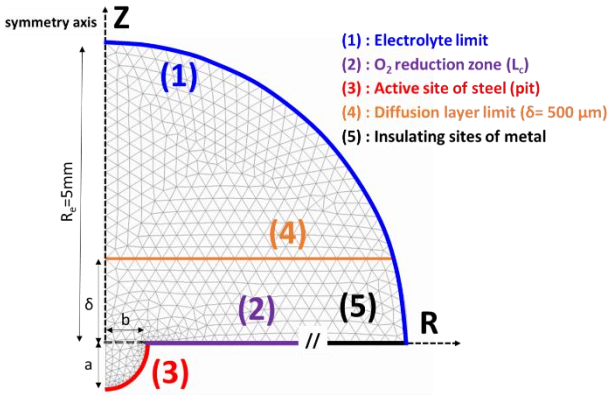

Figure 1 – Corrosion pit geometry

Electrochemical kinetics

The electrochemical reactions considered are:

- Iron (II) and chromium (III) oxidation within the active site of steel
- Reduction of chemical species near the corrosion pit: proton, water, and oxygen

These half-reactions as well as their current densities and standard potential are given in **Table. 3**

Half-reactions	Current density (A.m^{-2})	E^0 (V/SCE)
$Fe \rightarrow Fe^{2+} + 2e^-$	$i_{a,Fe^{2+}} = i^0_{a,Fe^{2+}} . \frac{c_{H^+}}{c_0} . \exp\left(\frac{\alpha_{Fe^{2+}} . F}{RT} \left((\varphi_m - \varphi_L) - E^0_{Fe^{2+}/Fe} \right) \right)$	− 0,682
$Cr \rightarrow Cr^{3+} + 3e^-$	$i_{a,Cr^{3+}} = i^0_{a,Cr^{3+}} . \frac{c_{H^+}}{c_0} . \exp\left(\frac{\alpha_{Cr^{3+}} . F}{RT} \left((\varphi_m - \varphi_L) - E^0_{Cr^{3+}/Cr} \right) \right)$	− 0,982
$H^+ + e^- \rightarrow \frac{1}{2} H_2$	$i_{c,H^+} = -i^0_{c,H^+} . \left(\frac{c_{H^+}}{c_0} \right)^{0,5} . \exp\left(-\frac{\alpha_{H^+} . F}{RT} \left(\varphi_m - \varphi_L - E^0_{H_2/H^+} \right) \right)$	− 0,242
$H_2O + e^- \rightarrow \frac{1}{2} H_2 + OH^-$	$i_{c,H_2O} = -i^0_{c,H_2O} . \exp\left(-\frac{\alpha_{H_2O} . F}{RT} \left(\varphi_m - \varphi_L - E^0_{H_2O/OH^-} \right) \right)$	−1.078
$O_2 + 2H_2O + 4e^- \rightarrow 4OH^-$	$i_{c,O_2} = -i^0_{c,O_2} . \left(\frac{c_{O_2}}{c_0} \right) . \exp\left(-\frac{\alpha_{O_2} . F}{RT} \left(\varphi_m - \varphi_L - E^0_{O_2/OH^-} \right) \right)$	0.158

Table. 3 - Current density and standard potential associated to each of the half-reactions

Each of the current densities mentioned before has two unknown parameters: **apparent current density ($i^0_{a,c}$) and Charge transfer coefficient ($\alpha_{a,c}$)**. These parameters were obtained thanks to the experimental work done by Naval Group: a parametric study was conducted to fit the polarization curve resulting from numerical simulation with the experimental curve. The results of the parametric study will be presented in the following section. In **Table. 3**, φ_m and φ_L represent the electrical potential (with respect to saturated calomel electrode SCE) of the steel and the electrolyte, respectively. A limit current density given by the following equation was also applied for the oxygen:

$$i^{lim}_{co_2} = \frac{4.F.D_{O_2}.c_{O_2}}{\delta} \qquad \textbf{Eq.5}$$

Chemical evolution of the medium/electrolyte

The chemical reactions taking place in the medium will be considered at equilibrium state. The list of chemical reactions presented in **Table. 4** is not exhaustive, however, other chemical reactions could be implemented into the numerical model if needed.

Reactions	Thermodynamic data (25°C)
$Fe^{2+} + H_2O = FeOH^+ + H^+$	$pK_{FeOH^+} = 9,5$
$Cr^{3+} + H_2O = Cr(OH)^{2+} + H^+$	$pK_{Cr(OH)^{2+}} = 3,42$
$Fe^{2+} + Cl^- = FeCl^+$	$pK_{FeCl^+} = -0,14$
$H_2O = H^+ + OH^-$	$pK_w = 14$

Table. 4 - Chemical reactions and associated thermodynamic constants

Modelling of pit propagation

Electrochemical dissolution of 316L steel (iron and chromium oxidation) can lead to a propagation of the corrosion pit. In this work, only pit evolution over the time is studied: neither depassivation nor passivation / repassivation of steel are considered. Thus, under COMSOL Multiphysics®, "deformed Geometry" interface was used to model corrosion pit propagation. This latter is dependent on the corrosion velocity (kinetics) which is referred as v_{corr} and given by:

$$v_{corr}(\mu m/y) = \frac{i_{a,Fe^{2+}}}{2.F} . \frac{M_{Fe^{2+}}}{\rho_{Fe^{2+}}} + \frac{i_{a,Cr^{3+}}}{3.F} . \frac{M_{Cr^{3+}}}{\rho_{Cr^{3+}}} \qquad \textbf{Eq.6}$$

With $i_{a,i}$ anodic current density (A.m^{-2}), F Faraday constant (96500 C.mol^{-1}), M_i molar mass (kg.mol^{-1}) and ρ_i the density (kg.m^{-3}). Symbol "i" refers to each of the oxidizing species (iron and chromium)

The initial and boundary conditions are quite intuitive: apart from the pit boundary **(3)**, all the other boundaries are fixed. Therefore, velocity and displacement conditions are presented in **Figure *2***. Radial and vertical displacement are referred as dR and dZ, respectively. It should be noted that corrosion velocity is imposed according to the normal $\vec{n}$ of the pit boundary. Two points "a_1" and "b_1" will be introduced to study the evolution of the pit in the vertical (Z direction) and horizontal directions (R direction), respectively. This will prove whether the pit displacement is greater at the surface than at depth.

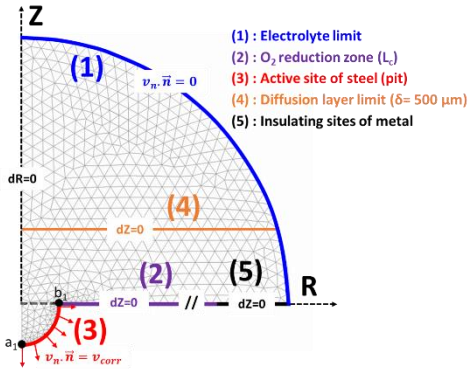

Figure 2 – Boundary conditions for pit propagation/deformation

Pit deformation will lead to a geometry (shape and size of the pit) which may vary over the time. For this reason, "Moving Mesh" functionality was used with an automatic remeshing of the geometry.

III. Results

Electrochemical kinetics parameters

An experimental study was realized by Naval Group to determine ($\mathbf{i^0_{a,c}}$) and ($\boldsymbol{\alpha}_{\mathbf{a,c}}$) for 316L steel in a marine solution (pH=8 and 0.5M NaCl). Polarization curve has been measured experimentally, and then, a parametric study was conducted numerically to identify ($\mathbf{i^0_{a,c}}$) and ($\boldsymbol{\alpha}_{\mathbf{a,c}}$) by fitting the experimental curve. The parameters identified in **Table. 5** are valid for a polarization potential between -1.2 V/SCE and 0.25 V/SCE. The free corrosion potential is about -0.14 V/SCE. For an applied potential that exceed 0.25 V/SCE, steel

depassivation will occur and current densities will reach higher value due to the corrosion initiation.

Half-reactions	α	i^0 ($A.m^{-2}$)
$Fe \rightarrow Fe^{2+} + 2e^-$	0.2	147
$Cr \rightarrow Cr^{3+} + 3e^-$		2.8
$H^+ + e^- \rightarrow \frac{1}{2}H_2$	0.35	1.084
$H_2O + e^- \rightarrow \frac{1}{2}H_2 + OH^-$		10.08 x10^{-2}
$O_2 + 2H_2O + 4e^- \rightarrow 4OH^-$	0.98	2.77 x10^{-6}

Table. 5 - ($i^0_{a,c}$) and ($\alpha_{a,c}$) resulting from parametric study

Numerical results

The aim of this section is to study the effect of the initial shape of the pit and the applied potential on the pit propagation for a period of 30 years. The following steel potentials were applied (vs SCE electrode) in the numerical simulation: -0.14 (free corrosion potential), -0.1, 0, 0.1 and 0.15 V/SCE.

a) Ellipsoid pit with a=100 µm and b=5µm

An example of a corrosion pit with an initial semi-ellipsoidal shape is presented in **Figure 3** when a steel potential of 0.15V/SCE was applied for a period of 30 years. It is clearly seen that corrosion phenomenon is taking place with a more acidic pH near and inside the pit. In this case (0.15 V/SCE), the propagation of the pit bottom (vertical displacement at a_1=48.4µm) is greater than the horizontal displacement at the pit mouth (horizontal displacement at b_1=41.9µm). In addition, initial semi-ellipsoidal shape is not preserved since the Z axis is closer to the lower part of the pit (horizontal distance of 45.9 µm) in comparison with the pit mouth (horizontal distance of 41.9+b=46.9 µm).

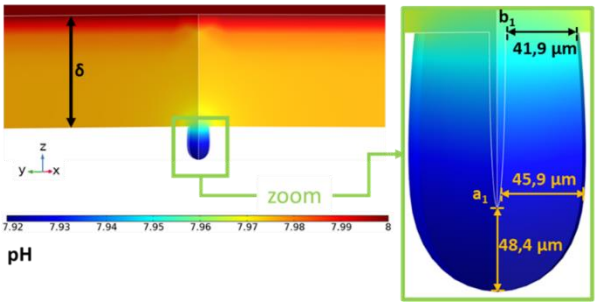

Figure 3 -Numerical simulation showing pH distribution and pit's shape after 30 years; 0.15 V/SCE

The parametric study with steel potential variation (**Figure 4**) showed a displacement that increases with the applied potential due to the migration effect. In addition, steel potential does not control only displacement magnitude but also its direction. For a free corrosion system (-0.14 V/SCE), horizontal displacement (a_1) at the top of the pit exceed the vertical displacement at its bottom (b_1): after 30 years, the displacement difference is about 0.61µm (3.9 v/s 3.29 µm). The same behavior was observed in the case of -0.1 V/SCE but the displacement difference decreases to about 0.2µm (5.65 v/s 5.45µm) despite the fact that a higher potential was applied (-0.10 V/SCE). An increase of the potential to more anodic values (0 and 0.15 V/SCE) showed a behavior change with a more important displacement at the bottom level of the pit (the pit tends to widen) in comparison with the pit mouth. As mentioned before, the elliptical shape does not persist over time and the pit tend to "egg-shape" : this is clearly visible in the case of 0.15V/SCE (**Figure 4**).

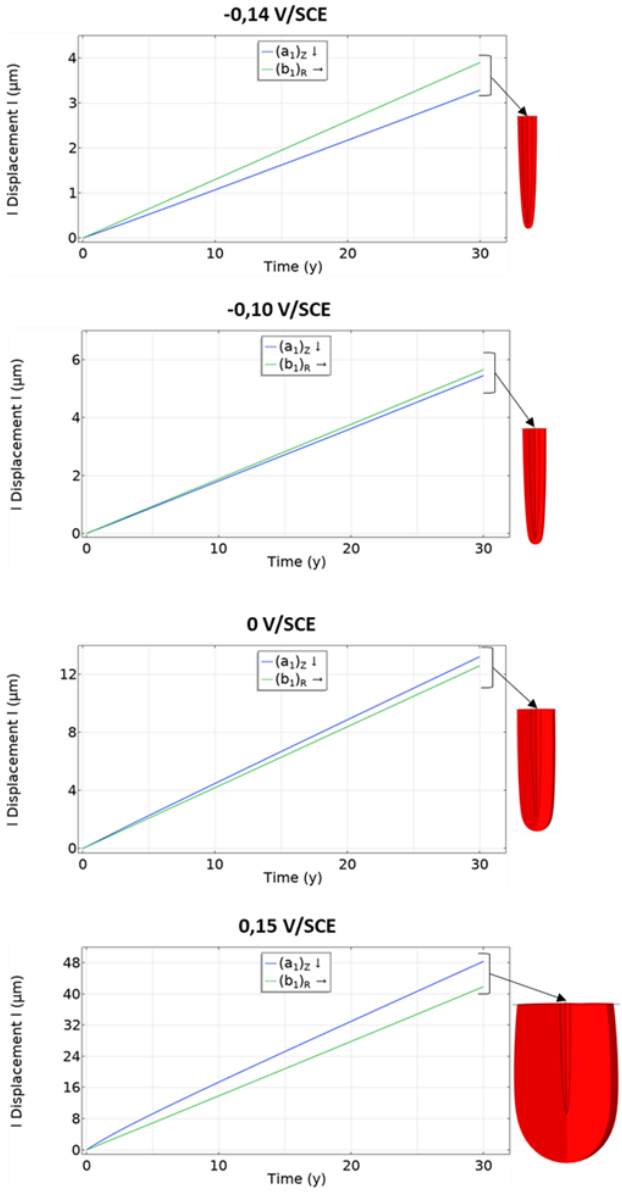

Figure 4 – Horizontal and vertical displacement at the mouth (b_1) and bottom (a_1) of the ellipsoid pit, respectively

b) Two Hemispherical pits with a radius of 5 and 100µm, respectively

The same parametric study was carried on again, but this time with a hemispherical pit using the same steel potential values. The results showed a closer displacement at the top (radial displacement $(b_1)_R$) and the bottom (vertical displacement $(a_1)_Z$) of the pit in comparison with the previous case (ellipsoid). In addition, regardless of the radius of the hemisphere (5 or 100µm), displacements (**Figure 5** and **Figure 6**) remains closer to the radial displacement calculated for ellipsoidal pit (**Figure 4**). After 30 years, the pit shape visually looks like a hemisphere as presented in **Figure 5** and **Figure 6**. This point will be discussed in the following section.

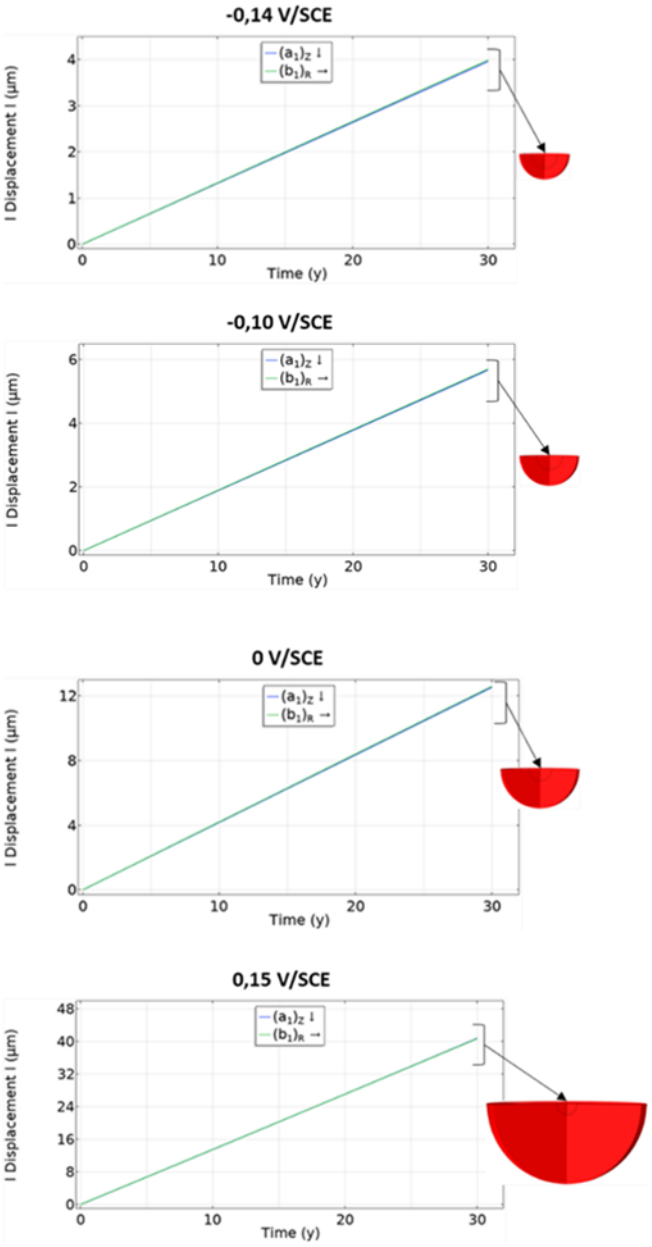

Figure 5 – Horizontal and vertical displacement at the mouth (b_1) and bottom (a_1) of the hemispheric pit, respectively, radius=5µm

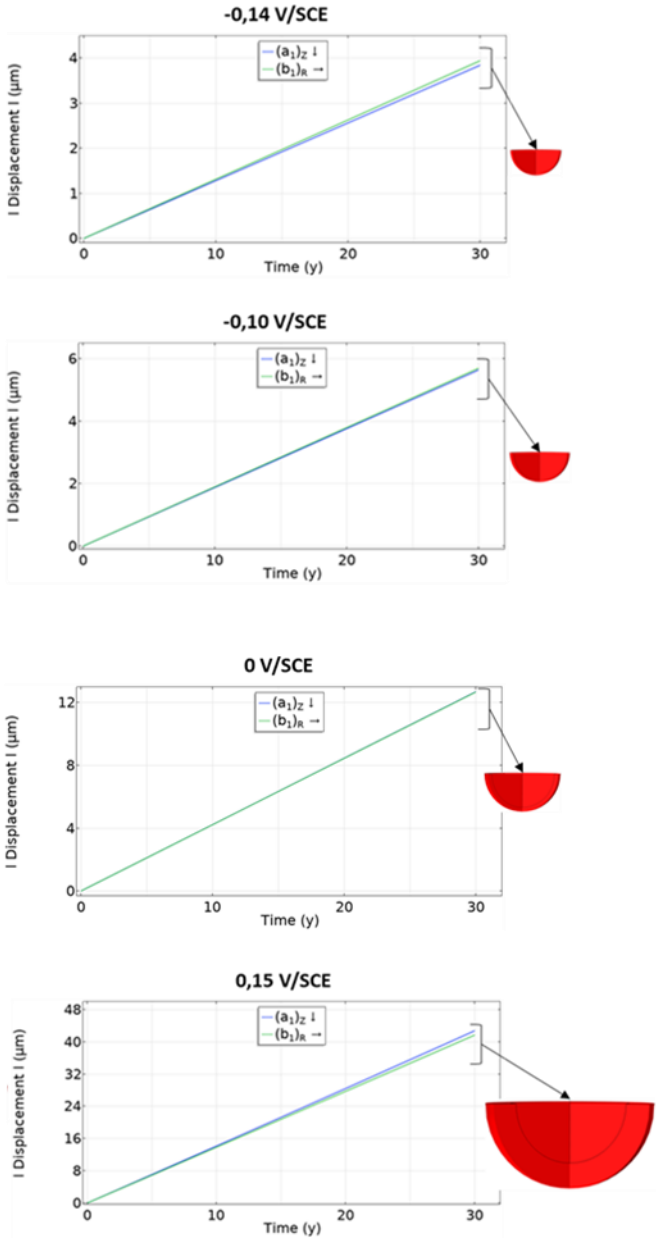

Figure 6 – Horizontal and vertical displacement at the mouth (b_1) and bottom (a_1) of the hemispheric pit, respectively, radius=100µm

c) Discussion

To compare the evolution of the pit shape during the time, the relative difference parameter was used. It is defined as follow:

$$\text{relative difference } (\%) = \left|\frac{(b_1)_R - (a_1)_Z}{\text{Min}\,((b_1)_R\,,(a_1)_Z)}\right| \qquad \textbf{Eq.7}$$

As presented in **Table. 6**, for a defined potential value, the highest relative difference is calculated for the ellipsoidal pit which shows the behavior of this kind of corrosion pit. It should be noted that relative difference values written in red (**Table. 6**) referred to the situation when $(a_1)_Z$ is higher than $(b_1)_R$. So, for a high anodic polarization (higher than 0 V/SCE, except for 5µm pit), the pit tends to propagate inside the steel, in the z-negative direction.

A 5 µm hemispherical pit has a very negligible value of relative difference (lower than 1%): so the assumption of shape conservation for an initial hemispherical pit can be accepted. For a bigger pit with 100µm radius, this hypothesis may not be valid especially for a free corrosion system (-0.14V/SCE) or when a high anodic polarization was applied. However, initial radius of a hemispherical corrosion pit is often limited to a few tens of micrometer: so, for this order of magnitude, the following assumption "hemispherical corrosion pit preserve its shape during corrosion process" is valid.

	Potential (V/SCE)	-0,14	-0,1	0	0,15
Ellipsoiid	$(b_1)_{R\rightarrow}$ (µm)	3,90	5,65	12,60	41,89
	$(a_1)_{Z\uparrow}$ (µm)	3,29	5,45	13,23	48,39
	Relative difference (%)	18,69	3,75	4,97	15,52
Hemisphere 5µm	$(b_1)_{R\rightarrow}$ (µm)	3,99	5,71	12,61	40,76
	$(a_1)_{Z\uparrow}$ (µm)	3,96	5,68	12,55	40,83
	Relative difference (%)	0,73	0,53	0,45	0,17
Hemisphere 100µm	$(b_1)_{R\rightarrow}$ (µm)	3,94	5,69	12,68	41,67
	$(a_1)_{Z\uparrow}$ (µm)	3,84	5,64	12,70	42,74
	Relative difference (%)	2,57	0,99	0,13	2,56

Table. 6 - Relative difference between $(b_1)_R$ and $(a_1)_Z$ for different pits with respect to the steel potential

IV. Conclusion

A 2D Numerical model was presented to simulate the growth of a corrosion pit for a 316L grade stainless steel using COMSOL Multiphysics® software. An interest is given to the numerical simulation results since an experimental study for this length of time is almost impossible. In addition, quantitative comparison between experimental and numerical results is complicated to realize especially with displacements of the order of few micrometers (precision of experimental measurements). The parameters implemented in the model results from an experimental study realized with a 316L grade stainless steel sample subjected to the same environmental conditions. Two shapes of pit have been tested: a hemispherical and ellipsoidal pit with the same medium. This study showed that corrosion pit growth depends on the electrical potential and the pit initial shape. An elliptical pit shape does not persist over time and the pit tend to "egg-shape". The assumption of shape conservation for an initial small hemispherical (radius of few micrometers) pit can be accepted. The behavior is different for a bigger hemispherical pit with more important radius (100µm).

V. Reference

[1]« N.J. Laycock and S.P. White, "Computer simulation of single pit propagation in stainless steel under potentiostatic control", J ELCHEM SO, 148(7), 2001, pp. B264-B275 ».

[2]« Scheiner S., Hellmich C., Computer Methods in Applied.Mechanics and Engineering 198 (2009) p.2898-2910 ».

[3]« Z. Zhu, N. Tajallipour, P.J. Teevens, H. Xue, and F.Y.F. Cheng. "A mechanistic model for predicting localized-pitting corrosion in a brine water-CO2 system", CORROSION, paper no. 256, (Houston, TX:NACE International, 2011) ».

[4]W. Mai, S. Soghrati, et R. G. Buchheit, « A phase field model for simulating the pitting corrosion », *Corros. Sci.*, vol. 110, p. 157-166, sept. 2016, doi: 10.1016/j.corsci.2016.04.001.

[5]« S.Salleh (2012), Modelling Pitting Corrosion in Carbon Steel Materials, UNIVERSITY OF MANCHESTER , England ».

[6]« S.Tricoit (2012), Modélisation et simulation numérique de la propagation de la corrosion par piqûres du fer en milieu chloruré : Contribution à l'évaluation de la durabilité des aciers au carbone en conditions de stockage géologique, UNIVERSITE DE BOURGOGNE, France ».

[7]« Xiao Z., Jun H., Yuqi W., Maosheng Z., Zaoxiao Z., Rare Metal Materials and Engineering 44 (2015) p2347-2352 ».

[8]« H. Wang et E.-H. Han, "Computational simulation of corrosion pit interac-tions under mechanochemical effects using a cellular automaton/finite element model," Corrosion Science103, 305–311 (2016). »